Progress in Physics of Applied Materials 5 (2025), 53 – 59

Semnan University

Progress in Physics of Applied Materials

journal homepage: https://ppam.semnan.ac.ir/

Exploring the Effects of pH on the Morphology and Optical Characteristics of $ZnFe_2O_4$ Nanoparticles

Mahdiyeh Taherkhani [a], Mohammad Hossein Ehsani [a*], Reza Zarei Moghadam [b], Abbas Javadian [a]

[a] *Faculty of Physics, Semnan University, P.O. Box:35195-363, Semnan, Iran*

[b] *Physics Department, Faculty of Science, Arak University, Arak, 38156, Iran*

ARTICLE INFO

Article history:
Received: 20 January 2025
Revised: 5 February 2025
Accepted: 11 February 2025

Keywords:
ZnF_2O_4 Nanoparticles;
Co-Precipitation Method;
X-Ray Diffraction Pattern.

ABSTRACT

In this paper, $ZnFe_2O_4$ nanoparticles were synthesized using the co-precipitation method, aiming to investigate the effect of pH on their structural and optical properties. The synthesis was carried out at various pH levels of 7, 9, and 11, to explore how acidic and basic conditions can influence the characteristics of these nanoparticles. Structural analysis was conducted using X-ray diffraction (XRD), which allowed for a comprehensive understanding of the phase composition and crystallinity of the nanoparticles. The XRD results revealed that as the pH increased from 7 to 11, the diffraction peaks became broader, indicating a reduction in crystalline size, which is a common phenomenon attributed to increased defects within the crystalline structure. This size reduction corresponds with an increase in dislocation density and strain within the samples, suggesting that higher pH environments lead to more significant structural alterations. Optical properties were investigated using a UV-Vis spectrometer. The optical analysis showed a noteworthy trend: as the pH increased from 7 to 11, the absorption capacity of the $ZnFe_2O_4$ nanoparticles decreased. This reduction in absorption may imply a modification in band gap energy, which is crucial for potential applications in photonic devices and sensors.

1. Introduction

Spinel ferrites have garnered significant attention from the scientific community and industry alike, owing to their multifaceted applications that span across various domains, including but not limited to magnetic materials, energy conversion and storage, bio-medicine, as well as numerous catalytic processes [1]. The properties of these materials are profoundly influenced by their shape, size, and structure; particularly when the dimensions are scaled down to the nanometer range, material characteristics may diverge dramatically from those observed in their bulk counterparts. This deviation in behavior underscores the critical importance of controlled synthesis techniques aimed at producing nanostructured materials, which can unveil unique optical, electrical, magnetic, and catalytic properties that are conducive to advancing our understanding of the intricate structure-property relationship inherent in nanomaterials. A plethora of synthetic methodologies have been developed to fabricate ferrite nanomaterials with diverse architectures, including hydro-thermal and solvo-thermal approaches, sol–gel synthesis, and template-assisted methods [2-4]. For instance, innovative fabrication techniques have led to the successful creation of homogeneous hollow core–shell microspheres composed of spinel ferrites such as MFe_2O_4 (where M includes Zn, Co, Ni, and Cd), utilizing carbonaceous saccharide microspheres as templates [5]. In another impressive demonstration, submicrometer ferromagnetic ferrite spheres exhibiting single-crystalline structures have been synthesized via solvothermal methods, resulting in exceptional colloidal stability in aqueous solutions. Additionally, porous "timber-like" superstructures of $ZnFe_2O_4$ have been achieved through

* Corresponding author. Tel.: +98-912-3314981
E-mail address: ehsani@semnan.ac.ir

Cite this article as:
Taherkhani M., Ehsani M. H., Zarei Moghadam R., and Javadian A., 2025. Exploring the Effects of pH on the Morphology and Optical Characteristics of ZnFe2O4 Nanoparticles. *Progress in Physics of Applied Materials*, *5*(1), pp.53-59.DOI: **10.22075/PPAM.2025.36655.1129**

the calcination of zinc ferrioxalate precursors [6]. The material $ZnFe_2O_4$ has attracted considerable interest due to its applicability in a range of modern technological sectors, including magnetic materials, adsorption mechanisms, photocatalytic applications, and solar cells. For example, magnetic $ZnFe_2O_4$ nanoparticles have been utilized as colorimetric biosensors for urine glucose detection due to their intrinsic peroxidase-like activity. Moreover, $ZnFe_2O_4$ nanorods have demonstrated commendable photocatalytic efficiency in the degradation of methylene blue, highlighting their potential in environmental remediation [7-9]. Nevertheless, the controlled synthesis of ferrite nanomaterials that exhibit tunable morphologies, structures, and properties remains a formidable challenge in the field. Particularly noteworthy is the potential of magnetic nanomaterials, including the superparamagnetic iron series, for significant advancements in biomedical applications such as magnetic resonance imaging (MRI), separation and purification processes, targeted drug delivery mechanisms, and magnetically induced hyperthermia therapies. However, the prevalent limitation of low magnetization values in superparamagnetic materials hampers their practical utility in these applications, thereby underscoring the necessity for continued research and development in this burgeoning area of nanomaterials science. Sonia et al. prepared $ZnFe_2O_4$ nanoparticles using two methods: sol-gel and co-precipitation. The results show that the particle size was reduced using the co-precipitation method, and the band gap was about 2.76 eV in the co-precipitation method [5]. Sun et al. prepared zinc ferrite nanoparticles using a sol-gel method. They calcined the samples at different temperatures. The results showed that the particle size increased with increasing calcination temperature. They also showed that these nanoparticles could be used for photocatalytic applications [10].

In this study, $ZnFe_2O_4$ nanoparticles were synthesized using the co-precipitation method to investigate the effect of pH on their structural and optical properties. The samples were prepared at pH levels of 7, 9, and 11. To examine the structural properties and determine the phase type, X-ray diffraction (XRD) patterns were used. For the analysis of optical properties, a UV-Vis spectrophotometer was employed. The novelty of this paper lies in the systematic investigation of the effect of pH on the structural and optical properties of $ZnFe_2O_4$ nanoparticles synthesized via the co-precipitation method. For the first time, changes in crystallite size, dislocation density, and lattice strain at different pH levels (7, 9, and 11) were studied using X-ray diffraction (XRD). Additionally, variations in optical properties (light absorption and bandgap energy) were analyzed using UV-Vis spectroscopy. The results demonstrate that increasing the pH leads to a reduction in crystallite size and significant alterations in optical properties, which are crucial for applications in photonics and sensors. This study provides a new approach for controlling and optimizing the properties of $ZnFe_2O_4$ nanoparticles by tuning the pH during synthesis.

2. Experiment

2.1. Materials

In the present study, a variety of chemicals were employed, all of which were sourced from the Merck company, Germany, and were of analytical grade, ensuring a high degree of purity and reliability for laboratory applications. Specifically, the materials utilized included ferric chloride hexahydrate ($FeCl_3 \cdot 6H_2O$), zinc chloride ($ZnCl_2$), sodium hydroxide (NaOH), and ethanol, all of which were used as received without any further purification. Additionally, double-distilled water was used for all experimental procedures to maintain consistency and accuracy in the reactions conducted. This meticulous attention to material quality underscores the rigorous standards upheld throughout the experimental phases of the research.

2.2. Synthesis of $ZnFe_2O_4$ Nanoparticles

Magnetic nanoparticles were successfully synthesized through the co-precipitation method, employing a systematic approach to achieve the desired properties. Initially, 2.27 g of ferric chloride ($FeCl_3$) was combined with zinc chloride ($ZnCl_2$) in a nitrogen atmosphere, utilizing 200 mL of water within a three-neck flask. To ensure thorough mixing, the components were subjected to a magnetic stirrer. Subsequently, 4 g of sodium hydroxide (NaOH) was dissolved in 100 mL of water and added dropwise to the mixture while maintaining magnetic stirring. This process continued until the pH of the solution reached 10, after which it was subjected to stirring at 80°C for a duration of two hours. Following this, the resultant mixture was filtered using filter paper and washed with water and ethanol until a neutral pH of 7 was achieved. To facilitate the drying of the materials, they were placed in an oven at 100°C for 12 hours. Finally, synthesized materials corresponding to pH levels of 7, 9, and 11 were calcined in a furnace at 550 °C, ensuring the enhancement of their magnetic properties through thermal treatment.

2.3. Characterization

$ZnFe_2O_4$ nanoparticles underwent a systematic investigation using X-ray diffraction (XRD) with an ADVANCE–D8 model, utilizing CuKα radiation (λ = 1.5406 Å). Complementary analyses were conducted using a Field Emission Scanning Electron Microscope (FESEM) of the MIRA4 TESCAN model, as well as a UV-Vis spectrophotometer, specifically the PerkinElmer Lambda-950. These instruments provided valuable insights into the structural, morphological, and optical properties of the nanoparticles.

3. Result and Discussion

3.1. Structure Study

Figure 1 presents the X-ray diffraction (XRD) patterns of samples synthesized under varying pH conditions, specifically at pH levels of 7, 9, and 11, elucidating the structural properties inherent to these specimens.

Notably, all samples displayed a cubic crystalline structure aligned with the space group Fd-3m, confirming their consistency with the reference pattern identified in the JCPDS card number 2397-074-01 [10]. A meticulous analysis of the diffraction patterns reveals a significant trend correlated with the alteration of pH. The remaining peaks exhibited a marked sharpening effect, which is indicative of a reduction in crystallite size, suggesting the formation of nanometer-scale crystallites. This observation not only underscores the critical role of pH in modulating the crystallographic characteristics of the samples but also implies potential implications for the material's applications, as such size-dependent properties are often pivotal in determining the efficacy and performance of nanomaterials in various technological contexts.

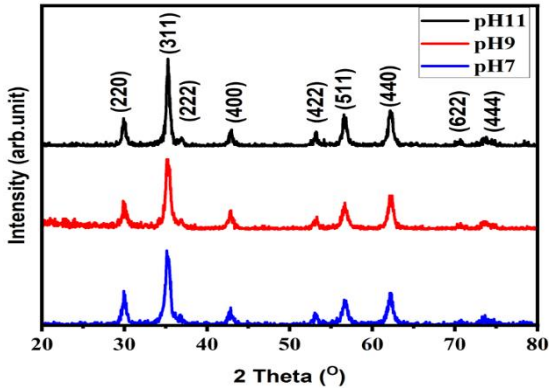

Fig. 1. XRD patterns of pH7, pH9 and pH11 samples

The crystallite size of the samples was calculated using the Debye-Scherrer formula [11]:

$$D_{XRD} = \frac{0.9\lambda}{\beta_{hkl}\cos(\theta_{hkl})} \quad (1)$$

where D_{XRD} is the crystallite size, θ is the diffraction angle, λ is the wavelength of the X-ray (1.5406 Å), and β_{hkl} is the half-width of the maximum peak (FWHM). The crystallite size for the (311) peak was calculated, and the results are presented in Table 1.

The dislocation density (σ) of the prepared samples was estimated using the following relation [12], and the results are shown in Table 1:

$$\sigma = 1/D^2 \quad (2)$$

The strain of the samples was calculated using the following relation [12], and the results are presented in Table 1:

$$\varepsilon = \beta \cos\theta/4 \quad (3)$$

The data presented in Table 1 elucidate a significant inverse relationship between pH levels and crystallite size within the tested samples, demonstrating that as the pH ascends from a neutral value of 7 to a more alkaline level of 11, there exists a corresponding reduction in the dimension of the crystallites. This phenomenon suggests that the chemical environment, closely tied to the pH, plays a pivotal role in influencing the growth and formation of crystalline structures. Moreover, the results further reveal a consequential increase in both dislocation density and strain concomitant with the decrease in crystallite size. Such findings imply that as the crystalline entities become smaller, the number of defects within the crystal lattice intensifies, manifesting in heightened dislocation density. Furthermore, this increase in dislocation density presumably contributes to an augmentation of internal strain within the material, highlighting a complex interplay between crystallite dimensions and the mechanical properties of the samples. Therefore, it may be inferred that the manipulation of pH not only governs crystallite size but also profoundly impacts the structural integrity and stability of the material, necessitating further investigation to understand the underlying mechanisms driving these observed phenomena [13]. By applying Bragg's law, the lattice parameters and unit cell volumes of the samples were successfully calculated. The analysis revealed that the lattice parameters for samples pH7, pH9, and pH11 were determined to be 8.442, 8.469, and 8.511 Å, respectively. Furthermore, the unit cell volumes for these samples were also calculated, resulting in values of 601.63, 607.43, and 616.51 $Å^3$ for samples pH7, pH9, and pH11, respectively. Also, the crystal size was measured using the Williamson-Hall equation:

$$D = \frac{K\lambda}{FWHM\ cos(\theta)} + \frac{4\varepsilon}{tan(\theta)} \quad (4)$$

According to the Williamson-Hall equation, the crystal size for samples pHp7, pH9, and pH11 were determined to be 48.5, 18.2, and 12.1 nm, respectively.

Table 1. Structural and Morphological parameters of pH7, pH9 and pH11 samples

	Cos (θ)	D_{XRD} (nm)	ε ($Lin^2\ m^2$)	σ (Lin/m^2)	< D_{FESEM} > (nm)	σ_D
pH7	0.961	40.7	0.003	0.0006	43.24	0.77
pH9	0.953	25.2	0.004	0.0015	34.47	0.99
pH11	0.952	11.5	0.009	0.0074	30.35	0.15

3.2. Morphology Characterization

FESEM was used to characterize the morphologies of the as-prepared $ZnFe_2O_4$ nanoparticles. Figure 2 displays FESEM images of $ZnFe_2O_4$ nanoparticles at pH levels of 7, 9, and 11. The images show that the nanoparticles have grown in clusters. The thickness of the nanoclusters was measured using Digimizer software (version: 4. 1. 1. 0, MedCalc Software). Then, the obtained data were fitted to a log-normal distribution formula [14].

$$f(D) = \left(\frac{1}{\sqrt{2\pi}\sigma D}\right) \exp\left[-\frac{ln^2\left(\frac{D}{D_0}\right)}{2\sigma^2}\right] \quad (5)$$

where D_0 and σ are the median thickness of the plates and data dispersions (obtained from Eq. (4)), respectively. The mean thickness < D > and standard deviation σ_D were determined by using the results obtained from fitting Eq. (4) as well as relations 5 and 6, as summarized in Table 1 [15].

$$< D >= D_0 \exp\left(\frac{\sigma^2}{2}\right) \quad (6)$$

$$\sigma_D =< D > [\exp(\sigma^2) - 1]^{1/2} \quad (7)$$

The results of Table 1 show that with increasing pH from 7 to 11, the size of nanoclusters decreases from 43.24 to 30.35 nm.

EDX analysis of $ZnFe_2O_4$ nanoparticles at pHs of 11 is shown in Fig. 3. The peaks in the EDX spectrum indicate the presence of the elements Zn, Fe, and O with no impurities and the results confirm a good atomic weight ratio. The weight percentages of different elements in the nanoparticles were measured to be 31.75, 52.34, and 15.92 for oxygen, iron, and zinc, respectively. The analysis presented in Figure 4 elucidates the spatial arrangement of components within the final structure, demonstrating a commendable distribution characterized by the absence of substantial agglomerates or voids. This observation is indicative of a well-formed material with optimized structural integrity. However, the presence of the localized concentrations of iron (Fe) suggests that clustering phenomena occurred during the synthesis of the $ZnFe_2O_4$ nanoparticles. Such behavior may have implications for the overall magnetic properties and performance of the nanoparticles, warranting further investigation to understand the underlying mechanisms and their potential effects on the functionality of the material [16, 17].

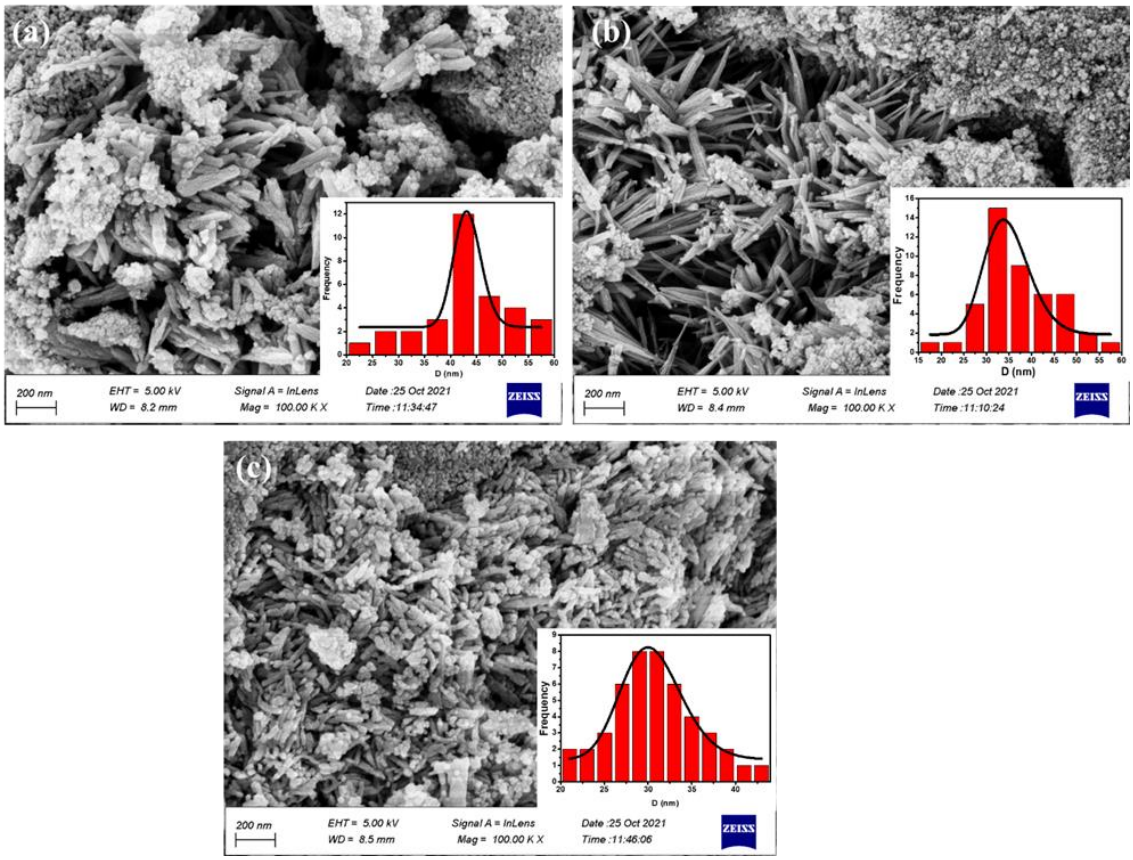

Fig. 2. FESEM images of $ZnFe_2O_4$ nanoparticles at pHs of 7 (a), 9 (b), and 11 (c)

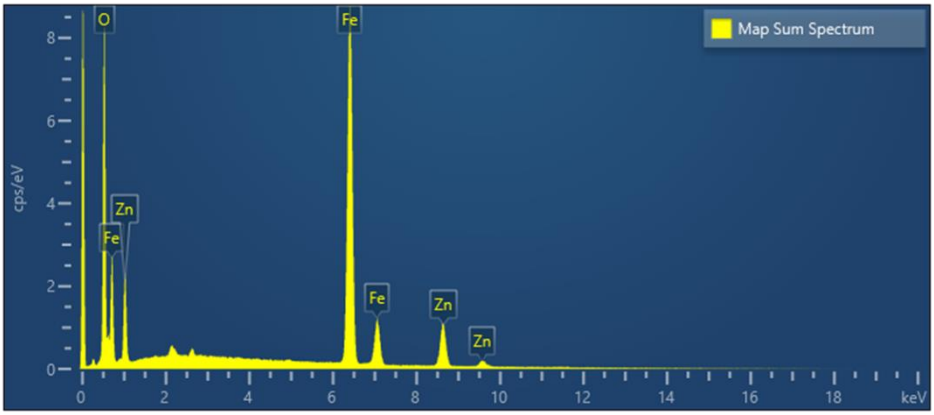

Fig. 3. EDX analysis of $ZnFe_2O_4$ nanoparticles at pHs of 11

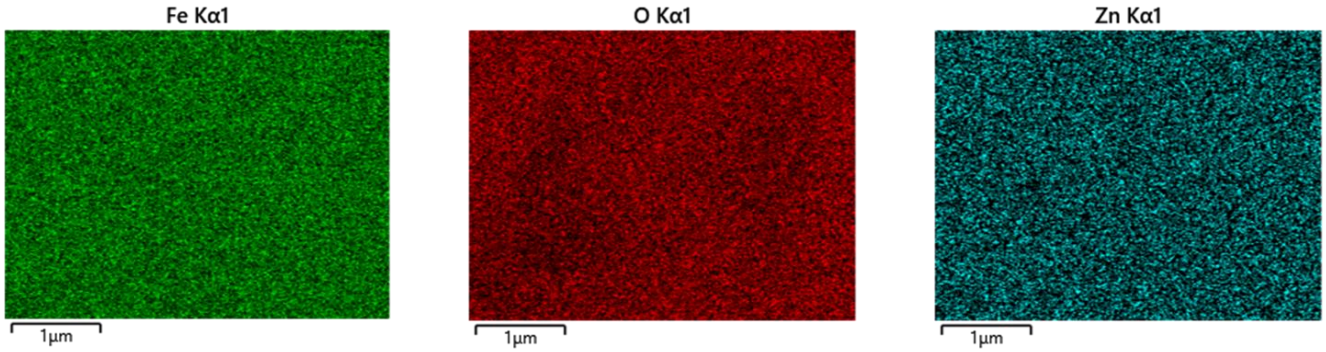

Fig. 4. Element mapping of $ZnFe_2O_4$ nanoparticles at pHs of 11

3.3. Optical Properties

The investigation into the optical properties of samples across varying pH levels was conducted utilizing a UV-Vis spectrometer, yielding significant insights into the relationship between pH and nanoparticle characteristics. As illustrated in Figure 5, the absorption spectra corresponding to samples at pH levels of 7, 9, and 11 demonstrate a clear trend: as the pH increases from 7 to 11, there is a concomitant decrease in the optical absorption of the samples, particularly noted alongside a reduction in nanoparticle size. This correlation suggests that both pH and particle dimensions play critical roles in influencing the optical behavior of the materials, thereby underscoring the importance of these parameters in the synthesis and application of nanomaterials in various fields [18].

The energy band gap, Eg, is calculated using the Tauc relation $\alpha hv=A(hv-Eg)$ q and by plotting the square of the absorption coefficient (α) against the incident energy (hv), where A represents the edge width parameter and q is a constant that equals 0.5 for ferrites, reflecting the type of transition [17]. In Fig. 6, the Tauc plot for all samples is presented, revealing that the optical energy band gaps are 2.51 eV for the pH7 sample, 2.26 eV for the pH9 sample, and 2.18 eV for the pH11 sample. Certain materials, particularly those with complex electronic structures (e.g., transition metal oxides like $ZnFe_2O_4$), may exhibit unique size-dependent properties that deviate from the typical quantum confinement trend. This behavior can arise from interactions between d-orbitals or spin-orbit coupling effects.

The observed decrease in the energy gap with reduced particle size can be explained by the dominance of surface states, lattice strain, and compositional changes, which introduce additional energy levels and modify the electronic structure of the material. This deviation from the typical quantum confinement trend highlights the complex interplay between size effects and material-specific properties in nanostructured systems [19, 20].

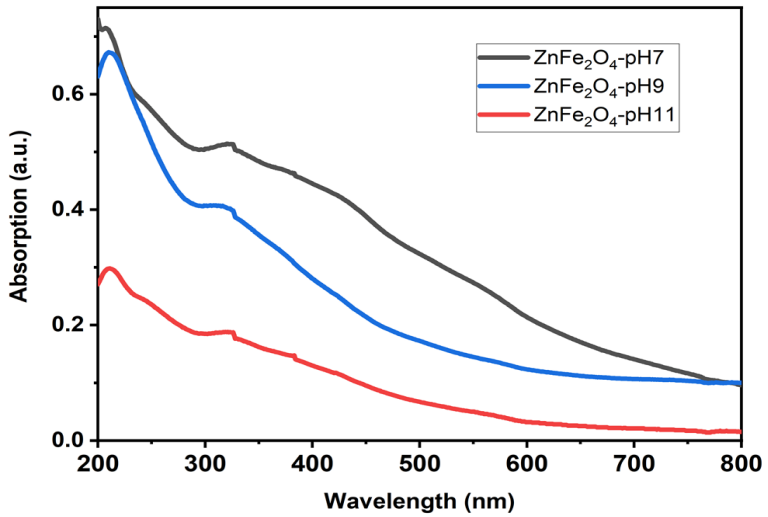

Fig. 5. The absorption spectra of $ZnFe_2O_4$ nanoparticles at pHs of 7, 9, and 11

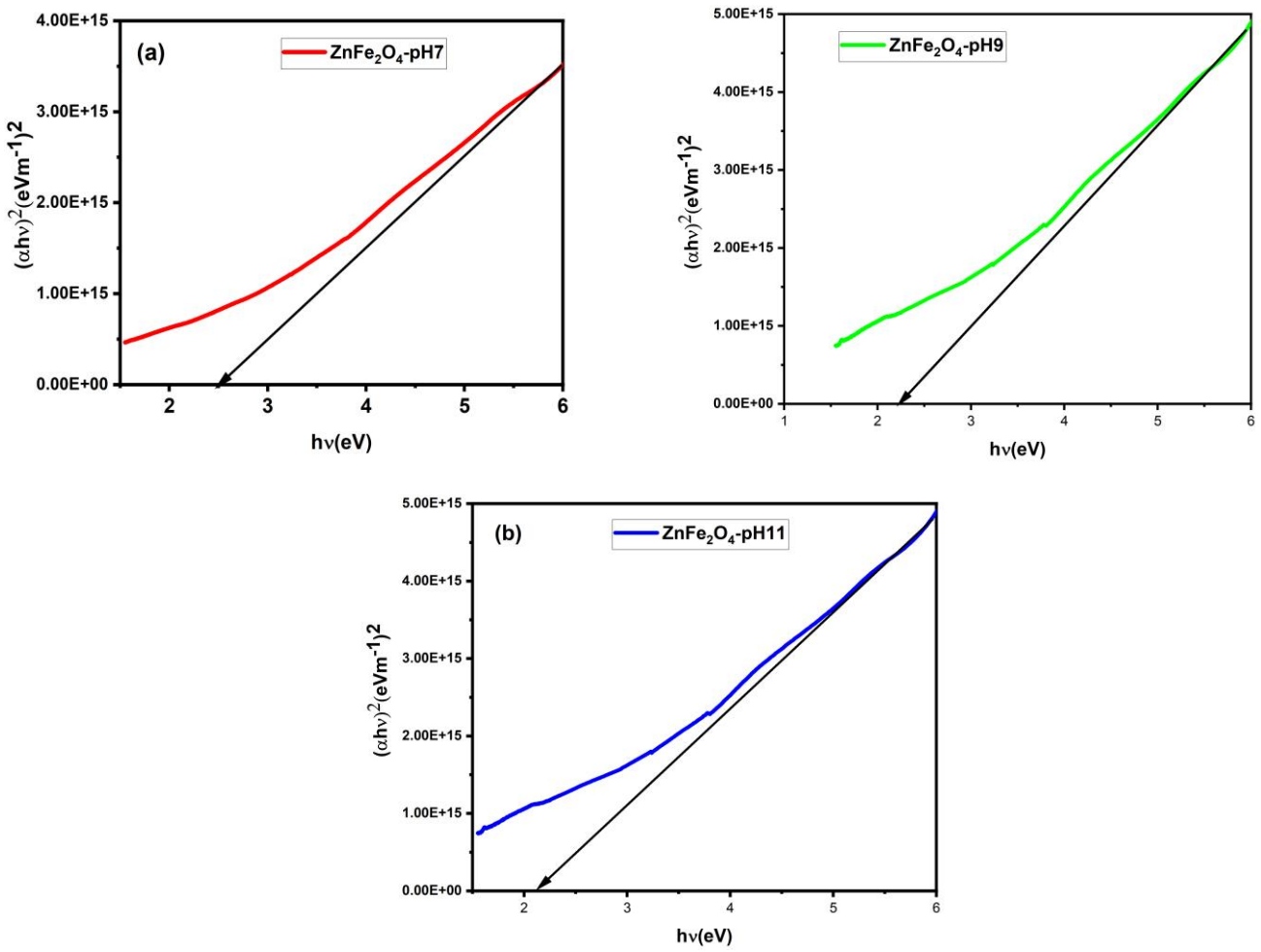

Fig. 6. The Tauc plots of $ZnFe_2O_4$ nanoparticles at pHs of 7, 9, and 11

4. Conclusions

In this study, $ZnFe_2O_4$ nanoparticles were produced at various pH levels using the co-precipitation technique. This method was chosen due to its straightforward sample preparation, brief reaction time, and rapid processing capabilities .The structural and morphological characteristics of the nanoparticles were examined through XRD and FESEM analyses. The stoichiometric composition of the synthesized nanoparticles was confirmed using EDAX analyses. The XRD patterns indicated that all samples crystallized in a cubic structure belonging to the space group Fd-3m. The average particle size of the samples ranged from 30 to 43 nm, with FESEM analysis revealing that an increase in pH value led to a decrease in nanoparticle size. Additionally, optical studies, which included calculations of band gap energy, indicated that the optical energy band gaps were 2.51 eV for the pH7 sample and 2.18 eV for the pH11 sample.

Conflicts of interest

Professor Mohammad Hossein Ehsani, the corresponding author of this paper is the current Director-in-Charge of Progress in Physics of Applied Materials (PPAM), but he has no involvement in the peer review process used to assess this work submitted to the Journal. This paper was assessed, and the corresponding peer review managed by Dr. Sanaz Alamdari, the Executive Manager of PPAM.

References

[1] Korkmaz, A.D., Güner, S., Slimani, Y., Gungunes, H., Amir, M., Manikandan, A. and Baykal, A., 2019. Microstructural, optical, and magnetic properties of vanadium-substituted nickel spinel nanoferrites. *Journal of Superconductivity and Novel Magnetism*, *32*, pp.1057-1065.

[2] Sharma, S., Kumar, D., Kumar, S., Goyat, M.S. and Mandal, P., 2018. Structural and optical properties of Cu incorporated ZnFe2O4 ferrite nanoparticles prepared by wet chemical route. *Materials Chemistry and Physics*, *212*, pp.292-297.

[3] Nanda, D., Kumar, P. and Prakash, C., 2017. Synthesis and characterization of Ni-Cu-Zn ferrites by microwave reactive sintering technique. *Integrated Ferroelectrics*, *185*(1), pp.183-192.

[4] Goya, G.F., Grazu, V. and Ibarra, M.R., 2008. Magnetic nanoparticles for cancer therapy. *Current nanoscience*, *4*(1), pp.1-16.

[5] Sonia, L.C., Victory, M. and Phanjoubam, S., 2020. A comparative study of the properties of zinc ferrite nanoparticles synthesized by different techniques for nanofluid preparation. *Integrated Ferroelectrics*, *204*(1), pp.100-111.

[6] Suppuraj, P., Thirunarayanan, G., Swaminathan, M. and Muthuvel, I., 2017. Facile synthesis of spinel nanocrystalline ZnFe2O4: enhanced photocatalytic and microbial applications. *Mater Sci Appl Chem*, *34*(1), pp.5-11.

[7] Vinosha, P.A., Mely, L.A., Jeronsia, J.E., Krishnan, S. and Das, S.J., 2017. Synthesis and properties of spinel ZnFe2O4 nanoparticles by facile co-precipitation route. *Optik*, *134*, pp.99-108.

[8] Iqbal, F., Abd Mutalib, M.I., Shaharun, M.S. and Abdullah, B., 2016. Synthesis of ZnFe2O4 using sol-gel method: effect of different calcination parameters. *Procedia engineering*, *148*, pp.787-794.

[9] Liu, R., Lv, M., Wang, Q., Li, H., Guo, P. and Zhao, X.S., 2017. Solvothermal synthesis of size-tunable ZnFe2O4 colloidal nanocrystal assemblies and their electrocatalytic activity towards hydrogen peroxide. *Journal of Magnetism and Magnetic Materials*, *424*, pp.155-160.

[10] Sun, Hao, He Cai, Linli Li, Yuan Yang, Pan He, Kun Zhou, Yu Han, Jie Guan, and Xiaoxing Fan. "Photothermal synergic catalytic degradation of the gaseous organic pollutant isopropanol in oxygen vacancies utilizing ZnFe2O4." *Journal of Chemical Research* 45 (9) 773-780 (2021).

[11] Ashrafi, M. Molla Ali, H. Rezagholipour Dizaji, M. H. Ehsani, and R. Zarei Moghadam. "ZnS Film properties modification using oblique angle deposition technique." *Surface Review and Letters* 25, no. 06 1850119 (2018).

[12] Moghadam, R.Z., Dizaji, H.R., Ehsani, M.H., Kameli, P. and Jannesari, M., 2019. Correlation study of structural, optical, and hydrophobicity properties of diamond-like carbon films prepared by an anode layer source. *Materials Research Express*, *6*(5), p.055601.

[13] Surendra, B.S., Nagaswarupa, H.P., Hemashree, M.U. and Khanum, J., 2020. Jatropha extract mediated synthesis of ZnFe2O4 nanopowder: Excellent performance as an electrochemical sensor, UV photocatalyst and an antibacterial activity. *Chemical Physics Letters*, *739*, p.136980.

[14] Moghadam, R.Z., Dizagi, H.R., Agren, H. and Ehsani, M.H., 2023. Understanding the effect of Mn2+ on Yb3+/Er3+ co-doped NaYF4 upconversion and obtaining the optimal combination of these tridoping. *Scientific Reports*, *13*(1), p.17556.

[15] Moghadam, R.Z., Dizaji, H.R., Ehsani, M.H., Kameli, P. and Jannesari, M., 2019. Correlation study of structural, optical, and hydrophobicity properties of diamond-like carbon films prepared by an anode layer source. *Materials Research Express*, *6*(5), p.055601.

[16] Surendra, B.S., Nagaswarupa, H.P., Hemashree, M.U. and Khanum, J., 2020. Jatropha extract mediated synthesis of ZnFe2O4 nanopowder: Excellent performance as an electrochemical sensor, UV photocatalyst and an antibacterial activity. *Chemical Physics Letters*, *739*, p.136980.

[17] Manohar, A., Vijayakanth, V. and Kim, K.H., 2021. Influence of Ca doping on ZnFe2O4 nanoparticles magnetic hyperthermia and cytotoxicity study. *Journal of Alloys and Compounds*, *886*, p.161276.

[18] Ahmed, A., Niazi, M.B.K., Jahan, Z., Ahmad, T., Hussain, A., Pervaiz, E., Janjua, H.A. and Hussain, Z., 2020. In-vitro and in-vivo study of superabsorbent PVA/Starch/g-C3N4/Ag@ TiO2 NPs hydrogel membranes for wound dressing. *European Polymer Journal*, *130*, p.109650.

[19] Alhusaiki-Alghamdi, H.M., 2024. Structural, Optical, Electrical, and Magnetic Characterization of PC/PEO Blend Incorporated with ZnFe2O4 Nanoparticles. *Advances in Polymer Technology*, 9443289 (2024).

[20] Li, Z.M., Wei, Z.Q., Ding, M.J., Yu, Q.S., Zhu, J., Bai, J.L. and Zhang, H.N., 2025. Photoelectrochemical and optical fenton properties of Cu-doped ZnFe2O4 composites synthesized by hydrothermal method. *Journal of Materials Science: Materials in Electronics*, *36*(2), pp.1-13.